DALTON
FULL PAPER

Quantum mechanical modelling of alkene hydroformylation as catalyzed by xantphos-Rh complexes †

Clark R. Landis * and Jamal Uddin

Department of Chemistry, University of Wisconsin, 1101 University Avenue, Madison, WI, USA. E-mail: landis@chem.wisc.edu

Received 25th September 2001, Accepted 20th November 2001
First published as an Advance Article on the web 29th January 2002

Fundamental issues concerning the hydroformylation of 1-alkenes as catalyzed by Rh complexes ligated with the xantphos diphosphine ligand are explored using ONIOM calculations. In this study xantphos serves as a prototype of the large bite-angle ligands that are associated with high regioselectivity and rates in catalytic hydroformylation. Computations have been used to explore the thermodynamics of 56 unique isomers (*e.g.*, *cis vs. trans* isomers of square planar complexes, diequatorial *vs.* axial-equatorial five-coordinate complexes) and conformers for intermediates along the reaction pathway. More than 20 transition states relevant to the catalyst mechanism have been determined. In terms of realistically modelling experiment, the computational results are mixed. In agreement with experiment, the computations yield a mixture of diequatorial and axial-equatorial isomers of $HRh(xantphos)(CO)_2$ as the catalyst resting state. Dissociation of CO from these complexes is computed to be barrierless leading to a computed free energy for exchange of CO ligands around 15 kcal mol^{-1}, somewhat lower than the value of *ca.* 20 kcal mol^{-1} derived from experimental data. The computed ratios of rates of propene insertion to form *n*-propyl and *i*-propyl Rh-alkyl (42 : 1) is in good agreement with experimental ratios of *n*-nonanal to *i*-nonanal (52 : 1) for 1-octene hydroformylation. Nonetheless, the computations dramatically overestimate the overall activation free energies for catalytic hydroformylation. Thus, at this stage computations do not provide useful insight into the the kinetics of hydroformylation and detailed mechanistic issues. It appears that much of this discrepancy between computed and experimental activation energies originates from the underestimation of propene bonding energies.

Introduction

Catalytic hydroformylation of simple alkenes, such as propene, in the presence of Rh catalysts is one of the largest volume applications of homogeneous, precious metal catalysts. Over the last twenty years, continued development of new phosphine and phosphite ligands has driven significant advances in hydroformylation chemistry, especially with respect to catalyst selectivity and stability.[1] A particularly useful development in the control of catalyst regioselectivity concerns the application of bulky diphosphines and diphosphites with wide bite angles[2] (Scheme 1): the larger the bite angle the greater the selectivity

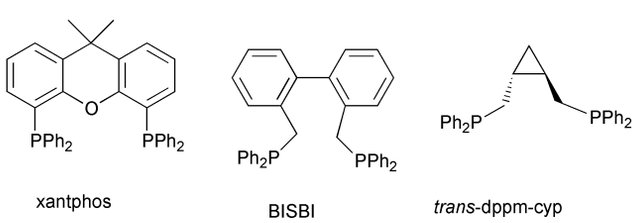

Scheme 1 Some large bite-angle diphosphines.

for linear aldehydes. New chiral diphosphines,[3] diphosphites,[4] and mixed systems[5] for enantioselective hydroformylations constitute another important, growing area of development.

The understanding of fundamental aspects of catalytic hydroformylation trails well behind the discovery of new and more effective catalysts.[1,6] Basic issues, such as the identities of the regioselectivity-determining and turnover-limiting steps, the speciation of catalyst among various isomers and complexes that lie within *vs.* outside of the catalytic cycle, and the molecularity (with respect to catalyst) of the aldehyde-producing step, are unclear at this point.[1] Further compounding these uncertainties is a paucity of reported kinetic data for the catalytic process, particularly with the more effective large bite angle bisphosphine and bisphosphite ligands.

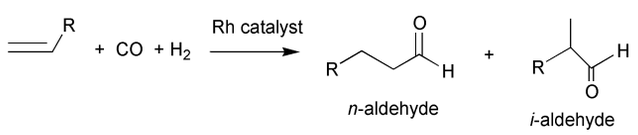

Many researchers have turned to computations in order to fill the voids in our understanding of catalytic hydroformylation.[7–12] The work of Morokuma and coworkers[9] focussed on complete quantum mechanical characterization of the hydroformylation of ethene in the presence of PH_3-ligated Rh. Very recently similar systems have been investigated by Decker and Cundari[10] using higher levels of theory (B3LYP/B3LYP and CCSD(T)/B3LYP). The first detailed computational analyses of bisphosphine ligands were reported by Gleich and coworkers.[11] These computations utilized a loosely coupled QM/MM approach. More recently, and of most relevance to this work, Carbó *et al.*[12] have employed tightly coupled QM/MM computational methods to examine the hydroformylation of ethene and propene using benzoxantphos and homoxanthpos ligands. These investigations provide the most detailed information to date on a realistic model catalyst system and the origins of regioselectivity.

Herein we report our initial findings of a large-scale computational project aimed at modelling propene hydroformylation as catalysed by Rh complexes containing the

† Based on the presentation given at Dalton Discussion No. 4, 10–13th January 2002, Kloster Banz, Germany.

DOI: 10.1039/b108649a

xantphos[13,14] ligand. One goal of this project is simply to explore whether computing a representative collection of intermediates, transition states, and their conformers for a realistic model of a multi-step catalytic process is reasonable. In this context, one criterion for feasability is the use of modern, easily accessible computational methods and hardware. A second goal is to establish the accuracy of the computational models *via* comparison with pertinent empirical data. Catalysts based on the xantphos ligand were chosen for this initial study because these catalysts exhibit high selectivity for linear aldehydes, good activities, and a relatively rich set of empirical data in the open literature. The ultimate goal of this project is the complete characterization of the free energy surface for hydroformylation *via* computations. From such studies we hope to sharpen our understanding of fundamental mechanistic issues. By coupling these computational models with a nascent experimental program exploring the kinetic and spectroscopic characterization of the catalytic process, we hope to develop enough constraints so as to resolve some of the basic mechanistic uncertainties mentioned above. This first report focuses on the structures and energetics of conformational and geometrical isomers of HRh(xantphos)$(CO)_2$ (**1**), HRh(xantphos)(CO) (**2**), HRh(xantphos)(CO)(propene) (**3**), (propyl)Rh(xantphos)(CO) (**4**), (propyl)Rh(xantphos)$(CO)_2$ (**5**), and (butanoyl)Rh(xantphos)(CO) (**6**) complexes and the transition states connecting these complexes and their various isomers.

Computational methods

All calculations were performed using the two-layered ONIOM[15–18] method as implemented in the Gaussian 98 program.[19] The calculations have been done wholly at the *ab initio* quantum mechanical level without the support of a molecular mechanics (MM) method. As a result, our calculations can be denoted as (High : Medium), where High is the level of theory on the core layer and Medium is the level on the whole system in generally accepted ONIOM formalism. All the species involved in the bond formation and bond breaking during the catalytic cycle of hydroformylation are designated as "core-layer" including two monodentate phosphine (PH_3) ligands as replacements for the bidentate xantphos ligand where the linked carbon atoms of xantphos are substituted with hydrogens. The idea is to reduce the computational costs while retaining the fundamental properties of the chelating xantphos ligand which is believed to control the regio- and stereoselectivity of the catalytic hydroformylation process.

All intermediates and the transition states have fully been optimized at (B3LYP/LANL2DZ : HF/LANL2MB) levels of theory where density functional (DFT),[20,21] with Becke's three-parameter functional (B3)[22] and Lee, Yang, and Parr (LYP)[23] correlation functional and Hartree–Fock theories have been utilized. For the core-layer, Hay and Wadt's LANL2DZ basis sets have been used with B3LYP and for the outer-layer, which includes the whole system, medium-level LANL2MB basis sets have been used and treated with HF theory. The LANL2DZ has a double-ζ quality basis set for the valence and penultimate shells, with effective core potentials at rhodium[24] and phosphorus,[25] and a Dunning/Huzinaga full double-ζ basis[26] on C, H, N and O. The outer-layer, which includes the whole system, has been treated with HF theory incorporation with LANL2MB basis sets which contain the same effective core potentials with a minimal basis set on the valence and penultimate shells of rhodium and phosphorus, plus minimal STO-3G basis sets[27] on C, H, and O. Computations have also been performed with the 'Stuttgart' basis sets and ECPs. The ECPs replaced 28 core electrons on rhodium and 10 on phosphorus. The Stuttgart valence basis sets have the following contraction schemes: (311111/22111/411) for rhodium[28] and (31/31) for phosphorus.[29] One d function with an exponent of 0.34 was added to phosphorus.[30] All other atoms used the 6-31G basis set.[31] All reported intermediates are true minima, as determined by the absence of any negative eigenvalue in the Hessian matrix in the vibrational frequency analysis of the potential energy surface. The located transition-state structures have a single negative eigenvalue (imaginary frequency) on the Hessian matrix as determined by using the synchronous-guided quasi-Newton (QST2 and QST3) methods as incorporated in Gaussian 98. All computations were performed on a 64-cpu cluster of Pentium III processors running under the LINUX operating system.

Results

A general working mechanism for the hydroformylation of propene as catalyzed by a Rh complex of xantphos is provided in Fig. 1. The catalytic cycle comprises two main branches: one for the production of the linear product, butanal, and one for the branched product, 2-methylpropanal. The species **1**, **2**, and **3** are common to both branches, with different isomers of **4** being produced at the branching point. A fundamental question, that will be only partly addressed in this paper, concerns whether the regioselectivity of propene hydroformylation is fixed upon alkene association (**2** ⟶ **3**), at the branching point (**3** ⟶ **4**), or at the subsequent CO insertion step (**4** ⟶ **5**). Although our working mechanism implies that the transformation **3** ⟶ **4** is irreversible and, hence, fixes the regioselectivity we emphasize that this is a simple convenience to be tested through computation, and ultimately, experiment.

Structures and thermodynamics of key intermediates

An aspect commonly bedevilling computations involving realistic models concerns the existence of many isomers and conformers. Although the xantphos ligand appears rather simple and rigid, we find a variety of conformational and geometric isomers as illustrated in Fig. 2. Three conformer classes of the xantphos ligand are populated; in the isomer with approximate C_2 symmetry the best-fit plane of the xantphos ligand lies nearly parallel with the P–Rh–P plane of the coordinated ligand. Two conformers with approximate C_s symmetry are found; they differ in the sense by which the non-planar xanthene array of fused cycles 'domes' or bends about the middle ring. One direction of bending places the O atom of the xanthene ring closer (proximal) to the Rh than the other (distal) direction.

Geometric isomers, also, abound. The xantphos ligand has a sufficiently large bite angle that *trans* arrangements in four coordinate complexes (*e.g.*, **2** and **4**) cannot be precluded. Although *trans* complexation at five-coordinate, trigonal bipyramidal complexes (*e.g.*, **1** and **3**) engenders too much steric crowding to persist, both the diequatorial (ee) and axial-equatorial (ae) dispositions of the xantphos P atoms give rise to low energy, true minima on the energy surface. Even further elaboration of isomers in the trigonal bipyramidal structures can be achieved by different positioning of, for example, the hydride, CO, and propene ligands of **3**

Descriptions of the structures of complexes **1**–**6** are presented below. Relative energies, enthalpies, entropies, and free energies of stable minima at 298 K as computed in this study are provided in Table 1. Our reference point for all relative energies is the most stable HRh(xantphos)(CO) isomer, **2a**. In the interest of brevity, we focus on the qualitative descriptions of the structures and relative energies for these complexes. Fine structural details of various isomers are tabulated but not discussed.

HRh(xantphos)$(CO)_2$ complexes (1). *In situ* spectroscopic studies of hydroformylation as catalyzed by bisphosphines similar to xantphos invariably reveal isomers of **1** as the only detectable species in solution.[14] We have located six minima

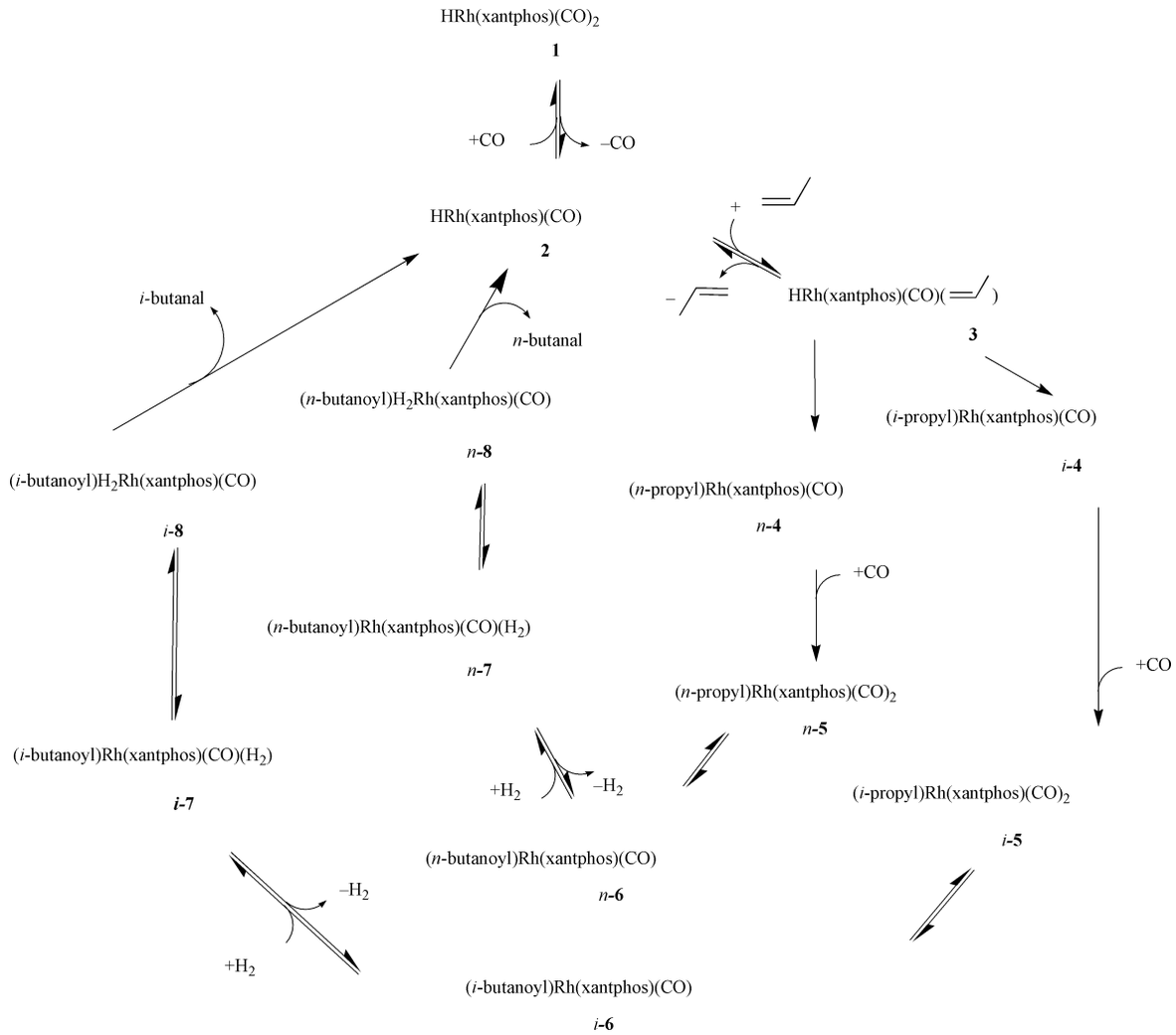

Fig. 1 A general mechanism for catalytic hydroformylation.

corresponding to isomers of **1** (see Fig. 3 and Table 2). Three of the isomers (**1a**, **1b**, and **1d**) correspond to axial-equatorial placements of the P atoms and the remaining isomers (**1c**, **1e**, **1f**) have diequatorial dispositions. All isomers have the H ligand in an axial position. Of the axial-equatorial isomers, the xantphos fragment of **1d** demonstrates a pseudo-C_2 symmetry whereas **1a** and **1b** exhibit pseudo-C_s symmetry of the xantphos fragment. For the diequatorial isomers, the xantphos fragment displays pseudo-C_s symmetry. The primary difference between **1b** and **1e** concerns the proximity of the H to the xanthene rings.

At this point in our search we find that the most stable isomer of five-coordinate HRh(xantphos)$(CO)_2$, **1a**, has an axial-equatorial disposition of P atoms. In terms of estimated free energies at 298 K, the most stable axial-equatorial isomer is about 1.3 kcal mol^{-1} more stable than the diequatorial isomer of lowest energy, **1c**. In contrast, experimental measurements of $^1J_{Rh-H}$ coupling constants at 298 K in benzene suggest that the diequatorial isomers predominate by a ratio of 7 : 3 ee : ae.[14] Given the uncertainties presented by both experiment and computation, perhaps the main conclusion to be drawn at this point is that diequatorial and axial-equatorial isomers of **1** are close in energy. From the computational side, a clear issue concerns finding all relevant conformers. For example, we have not yet located a diequatorial isomer of **1** that has a pseudo-C_2 symmetric conformation of the xantphos fragment. Given that **1a** has this conformation, the small discrepancy with experiment may reflect the absence of the most representative conformer of the diequatorial isomer from our current tabulation.

HRh(xantphos)(CO) complexes (2). Loss of CO from **1** yields the intermediate **2**. Of the six isomers of **2** that we have found (see Fig. 4 and Table 3), the three *cis* isomers (**2a**–**2c**) are lower in energy than the three *trans* isomers (**2d**–**2f**) by several kcal mol^{-1}. Despite the rather small ideal bite angle for the xantphos ligand (111°), *trans* configurations of the ligand have low enough energies that they could play a role in catalysis. The various *cis* isomers differ in the conformation of the xantphos fragment but are nearly isoenergetic.

The formation of **2** from **1** is thermodynamically uphill by *ca.* 15 kcal mol^{-1} in free energy under standard conditions. Correspondingly, one cannot expect **2** to be spectroscopically observable under catalytically relevant conditions. From computation, the bond dissociation enthalpy for loss of the first CO from **1** is estimated to be on the order of 26 kcal mol^{-1}. These values are a few kcal mol^{-1} higher than those found by others using PH_3 model complexes.[8–10]

HRh(xantphos)(CO)(propene) complexes (3). Addition of propene to **2** generates a large array of possible isomers and conformers of complex **3**. We have located a total of 16 minima for **3** (see Table 4 and Fig. 5). All but one of these minima, the structure **3o**, have the propene located *cis* with respect to the Rh–H bond. As a result, there are at least 15 minima that could be direct precursors to the crucial migratory insertion step in which the first C–H bond is formed. All structures of **3** conform well to trigonal bipyramidal geometry with the H always occupying an axial site. With the exception of **3o**, the propene is always coordinated such that the C=C bond vector lies in the equatorial plane.[9,10]

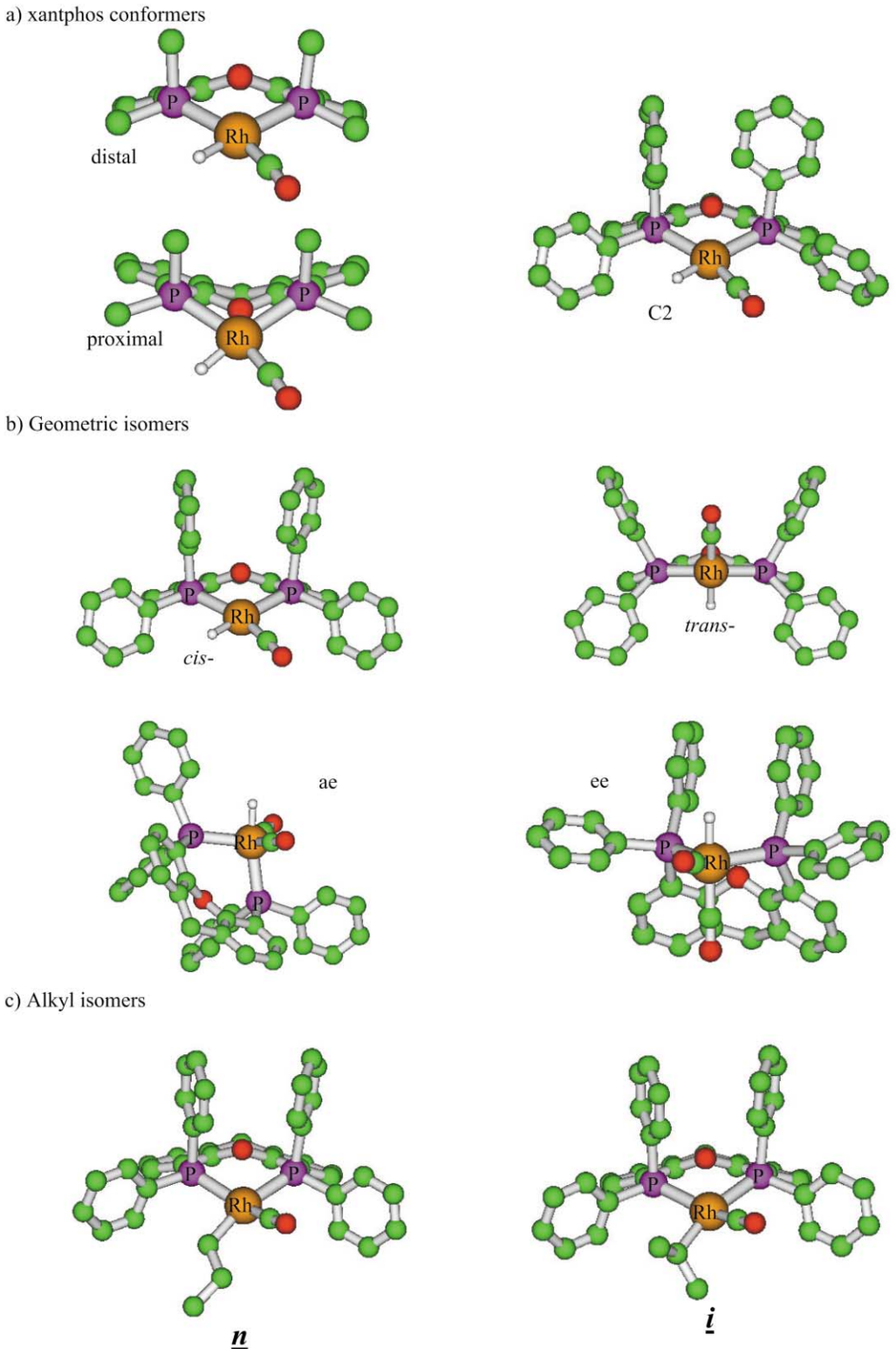

Fig. 2 Classes of isomers and conformers of intermediates.

Multiple examples of both axial-equatorial (**3a**–**3h**) and diequatorial (**3i**–**3p**) coordination modes are found. This complexity arises from the possibility of four different orientations of the propene ligand with respect to the Rh–H axis and from different conformations of the xantphos fragment. The most stable isomer of **3** with diequatorial disposition of the xantphos chelate, **3m**, is virtually isoenergetic with the axial-equatorial isomer. Thus the xantphos ligand is not computed to strongly favour either chelate mode for isomers of **1** or **3**.

Among the axial-equatorial isomers of **3**, the preferred orientation of the propene ligand (see **3a**) is that which places the methyl group of coordinated propene most remote to the sterically bulky groups. Rotation of propene to place the methyl group in the other three positions results in higher energies by about 1 kcal mol^{-1} increments in the order **3c**, **3d**, and **3e**.

The lone isomer with propene in an axial position, **3o**, cannot undergo direct insertion into the Rh–H bond without prior isomerization. The relatively high energy of **3o** indicates that significant pooling of catalyst into this species will not occur.

Binding propene to **2** to generate various isomers of **3** is weakly exothermic, at best. At the level of theory which we have employed, the most exothermic reaction releases just 0.9 kcal

Table 1 Thermodynamic values[a] for intermediates along the reaction pathway

	$\Delta H°$/kcal mol^{-1}	$\Delta G°$/kcal mol^{-1}	$\Delta S°$/cal mol^{-1} K^{-1}	ΔE/kcal mol^{-1}
1a	−26.15	−15.09	−37.09	−27.69
1b	−22.63	−11.75	−36.48	−24.04
1c	−25.07	−13.72	−38.07	−26.65
1d	—	—	—	−24.72
1e	−24.55	−13.39	−37.42	−26.19
1f	—	—	—	−22.03
2a	0.00	0.00	0.00	0.00
2b	0.55	0.51	0.14	0.59
2c	1.77	2.13	−1.20	1.71
2d	2.07	3.41	−4.47	2.03
2e	7.32	8.02	−2.36	7.27
2f	5.16	6.75	−5.33	5.19
3a	−0.91	13.82	−49.40	−2.56
3b	—	—	—	−0.72
3c	—	—	—	−1.53
3d	1.42	16.49	−50.54	−0.30
3e	2.13	17.39	−51.17	0.40
3f	2.92	18.19	−51.19	1.14
3g	—	—	—	2.86
3h	2.50	16.94	−48.44	0.92
3i	—	—	—	−0.40
3j	0.15	15.11	−50.20	−1.57
3k	1.54	16.49	−50.13	−0.33
3l	0.32	14.97	−49.14	−1.35
3m	−0.59	13.29	−46.55	−2.31
3n	0.64	14.76	−47.34	−1.22
3o	5.90	19.74	−46.43	4.17
3p	0.18	14.83	−49.13	−1.49
4a	−4.19	8.23	−41.70	−7.86
4b	−5.04	7.76	−42.97	−8.76
4c	−6.17	6.48	−42.45	−9.85
4d	−2.43	11.82	−47.80	−6.19
4e	0.55	13.28	−42.69	−3.05
4f	−4.14	9.02	−44.14	−7.89
4g	−1.63	12.23	−46.52	−5.29
4h	−2.54	10.37	−43.32	−6.11
4i	−3.96	9.43	−44.93	−7.45
4j	4.18	18.66	−48.58	0.57
4k	0.17	15.11	−50.09	−3.34
4l	3.66	18.59	−50.07	0.26
5a	−30.13	−5.18	−83.69	−35.49
5b	−30.65	−5.69	−83.73	−35.97
5c	−24.61	2.08	−89.54	−29.46
5d	−28.05	−4.11	−80.28	−33.49
5e	−28.46	−4.10	−81.69	−33.83
5f	−30.94	−7.44	−78.81	−36.35
5g	−28.30	−4.16	−80.96	−33.54
5h	−27.52	−2.22	−84.85	−32.67
5i	−28.12	−1.94	−87.82	−33.32
6a	−37.79	−14.61	−77.75	−44.21
6b	−38.55	−16.05	−75.47	−45.04
6c	−38.09	−13.93	−81.06	−44.63
6d	−39.22	−14.04	−84.42	−45.52
6e	−38.61	−15.42	−77.77	−45.02
6f	−38.69	−15.36	−78.26	−44.93

[a] All energies are relative to **2a** at 298 K.

Table 2 Geometric parameters computed for **1**

	Rh–H/Å	Rh–C1/Å	Rh–C2/Å	Rh–P1/Å	Rh–P2/Å	Bite angle/°
1a	1.586	1.905	1.906	2.516	2.555	103.2
1b	1.587	1.898	1.912	2.549	2.605	103.6
1c	1.609	1.935	1.892	2.482	2.482	105.3
1d	1.588	1.897	1.914	2.532	2.573	108.6
1e	1.613	1.936	1.891	2.485	2.485	107.0
1f	1.609	1.941	1.877	2.533	2.532	105.3

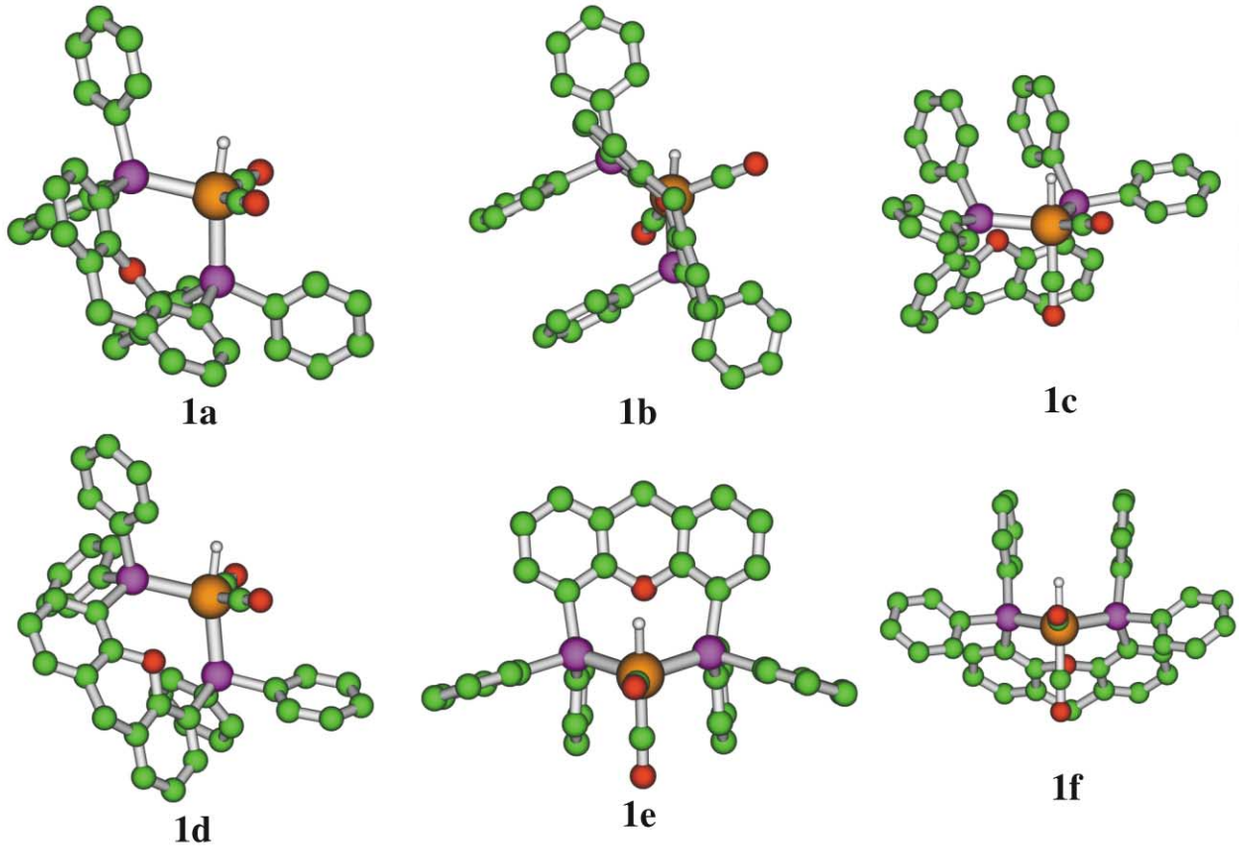

Fig. 3 Structures computed for isomers and conformers of **1**.

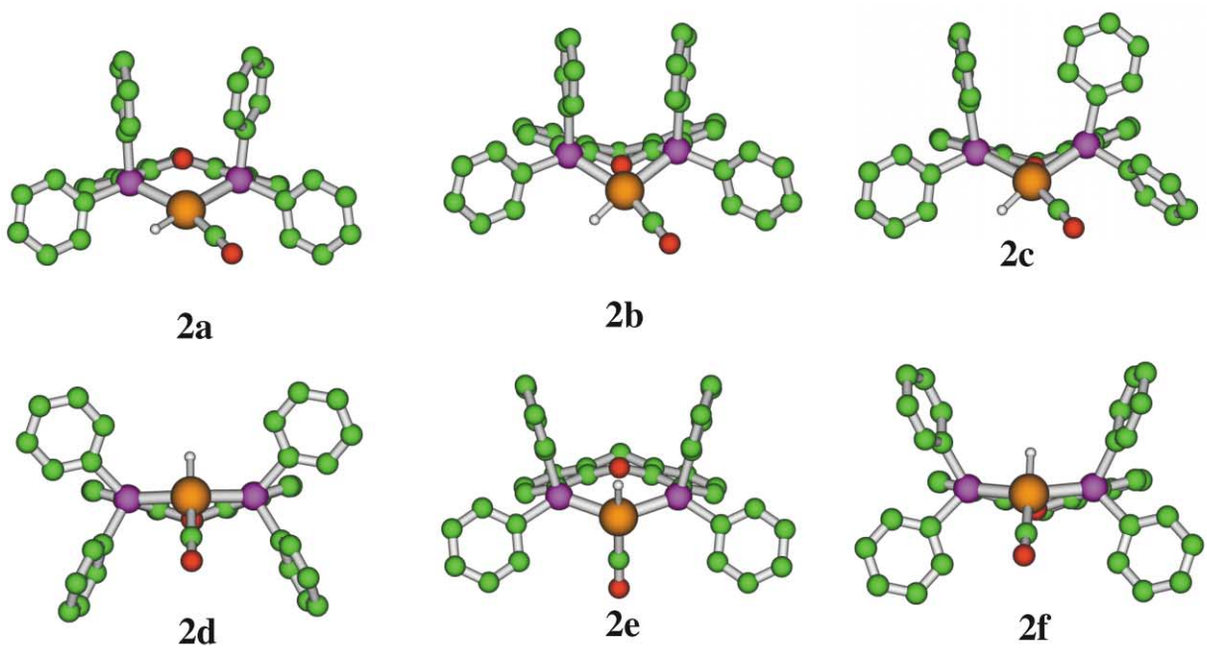

Fig. 4 Structures computed for isomers and conformers of **2**.

mol^{-1}. Given the unfavourable entropy of binding propene, the overall binding constant of propene to **2** is quite unfavourable. Hence, spectroscopically observable quantities of **3** should never accumulate. For comparison, the recent work of Decker and Cundari[10] reported exothermic (11–12 kcal mol^{-1}) binding of ethene to analogous model complexes using PH_3 as the phosphine ligand at the B3LYP level. However, and perhaps significantly for this work, the reaction was computed to be even more strongly exothermic (*ca.* 22 kcal mol^{-1}) at the CCSD(T)/B3LYP level. It is not surprising that the more realistic xantphos ligand model would create additional steric interactions that would disfavour coordination of alkene. However, the discrepancy of nearly 20 kcal mol^{-1} between our computations and those of Decker and Cundari raises serious concerns that the B3LYP model may be seriously underestimating the strength of the Rh–propene interaction.

(Propyl)Rh(xantphos)(CO) complexes (4). Migratory insertion of the alkene into the Rh–H bond transforms **3** into **4**. This process lends an additional degree of complexity to the overall analysis because both *i*-propyl (**4h–l**) and *n*-propyl (**4a–j**) groups can be produced. These structures are depicted in Fig. 6 and the

geometrical parameters are summarized in Table 5. Due to the four coordinate nature of **4**, the isomers may be further broken down into *cis* (**4a**,**b**,**h**–**j**) and *trans* (**4c**–**g**,**k**,**l**) models of diphosphine coordination.

Thermodynamically, the transformation **3** ⟶ **4** is slightly favourable (of the order of 1–6 kcal mol^{-1}), both in terms of enthalpy and free energy. As points of comparison, Decker and Cundari[10] report a 1–3 kcal mol^{-1} energy lowering upon insertion of ethene into a Rh–H bond and Morokuma and coworkers[9] report a potential energy increase of 4.2 kcal mol^{-1}. The most stable isomer, **4c**, is the *n*-propyl with *trans* xantphos coordination and the lowest energy *i*-propyl complex, **4i**, has a *cis*-disposition of the xantphos ligand. Formation of the *n*-propyl isomers is more favourable than formation of the *i*-propyl isomers by an increment of *ca.* 3 kcal mol^{-1}. However all isomers of **4** demonstrate strong distortions from ideal square planar coordination. Presumably this distortion reflects the inability of the xantphos ligand to achieve either 90 or 180° bite angles.

(Propyl)Rh(xantphos)(CO)$_2$complexes (5). Based on the exothermicity of the transformation **2** ⟶ **1**, one expects that the addition of CO to **4** should produce **5** with the release of significant heat. Such is the case as reaction enthalpies in the range of 25 kcal mol^{-1} are computed for formation of both the *n*-propyl (**5a**–**f**) and *i*-propyl isomers (**5g**–**i**) from **4** (see Table 6 and Fig. 7). Many of the energetic and structural features seen for the two previous five coordinate complexes, **1** and **3**, reappear in isomers of **5**. Namely, both diequatorial and axial-equatorial coordination modes are seen and are computed to have similar energies (for the *i*-propyl complexes the axial-equatorial mode has not yet been thoroughly searched). The *n*-propyl isomers are slightly more stable than the *i*-propyl isomers by the increment (*ca.* 3 kcal mol^{-1}) seen for **4**.

(Butanoyl)Rh(xantphos)(CO) complexes (6). Like the migratory insertion of the C=C double bond into a Rh–H bond, the computed insertion of CO into the Rh–propyl bond of **5** to yield butanoyl isomers (**6**) is mildly exothermic (*ca.* 7 kcal mol^{-1}) with similar values for the free energy. Values obtained by Decker and Cundari[10] for the analogous PH_3 model system average to about 9 kcal mol^{-1}. Six true minima of **6** (see Table 7 and Fig. 8) have been optimised and analyzed thermodynamically. Four of the minima are *n*-butanoyl isomers (**6a**–**d**) and two are the *i*-butanoyl isomers (**6e**,**f**). Although the sampling of the *i*-butanoyl isomers is rather limited at this point, it appears that the thermodynamic bias in favour of the *n*-propyl isomers computed for **5** largely disappears upon conversion to **6**. Presumably this reflects release of steric repulsions as the alkyl group is placed farther from the crowded metal center.

At this point we have computed 28 additional true minima corresponding to isomers of **7** and **8**. However, discussion of these intermediates and their free energies lies beyond the scope of this presentation.

Transition states and free energies of activation

Having established the relative thermodynamics of various potential reaction intermediates and their isomers and con-

Table 3 Computed geometric parameters for **2**

	Rh–H/Å	Rh–C/Å	Rh–P1/Å	Rh–P2/Å	Bite angle/°
2a	1.594	1.839	2.514	2.497	106.3
2b	1.591	1.835	2.508	2.519	104.8
2c	1.589	1.835	2.503	2.539	108.7
2d	1.651	1.894	2.347	2.347	146.1
2e	1.618	1.907	2.356	2.356	138.1
2f	1.655	1.887	2.349	2.349	144.1

Table 4 Geometric parameters computed for **3**

Isomer	Rh–H/Å	Rh–CO/Å	Rh–C1/Å	Rh–C2/Å	Rh–P1/Å	Rh–P2/Å	C=C/Å	Bite angle/°
3a	1.569	1.891	2.216	2.229	2.518	2.549	1.428	102.0
3b	1.565	1.888	2.232	2.226	2.526	2.579	1.426	105.7
3c	1.568	1.896	2.209	2.239	2.553	2.514	1.427	101.7
3d	1.568	1.888	2.222	2.258	2.265	2.535	1.424	101.0
3e	1.566	1.897	2.196	2.259	2.582	2.518	1.427	103.9
3f	1.569	1.893	2.208	2.264	2.588	2.517	1.424	106.2
3g	1.565	1.892	2.213	2.215	2.637	2.569	1.428	104.2
3h	1.569	1.889	2.232	2.235	2.600	2.555	1.422	106.7
3i	1.605	1.934	2.206	2.245	2.469	2.459	1.427	119.0
3j	1.615	1.926	2.216	2.242	2.449	2.469	1.425	117.9
3k	1.603	1.929	2.204	2.236	2.476	2.466	1.429	105.7
3l	1.608	1.927	2.204	2.245	2.464	2.484	1.427	105.7
3m	1.601	1.926	2.207	2.238	2.458	2.464	1.428	107.5
3n	1.611	1.926	2.207	2.234	2.467	2.485	1.428	106.7
3o	1.575	1.863	2.373	2.434	2.514	2.500	1.389	104.3
3p	1.617	1.924	2.211	2.236	2.461	2.463	1.427	111.95

Table 5 Geometric parameters computed for isomers of **4**

	Rh–C(R)/Å	Rh–CO/Å	Rh–P1/Å	Rh–P2/Å	Bite angle/°
4a	2.121	1.836	2.538	2.554	103.1
4b	2.131	1.831	2.571	2.542	102.9
4c	2.119	1.830	2.576	2.491	104.2
4d	2.181	1.878	2.374	2.374	144.9
4e	2.133	1.895	2.394	2.412	144.5
4f	2.154	1.893	2.385	2.388	135.2
4g	2.138	1.898	2.373	2.387	134.1
4h	2.145	1.837	2.549	2.563	102.8
4i	2.141	1.833	2.562	2.530	102.2
4j	2.187	1.884	2.384	2.409	142.3
4k	2.166	1.895	2.403	2.387	133.3
4l	2.154	1.898	2.382	2.414	139.1

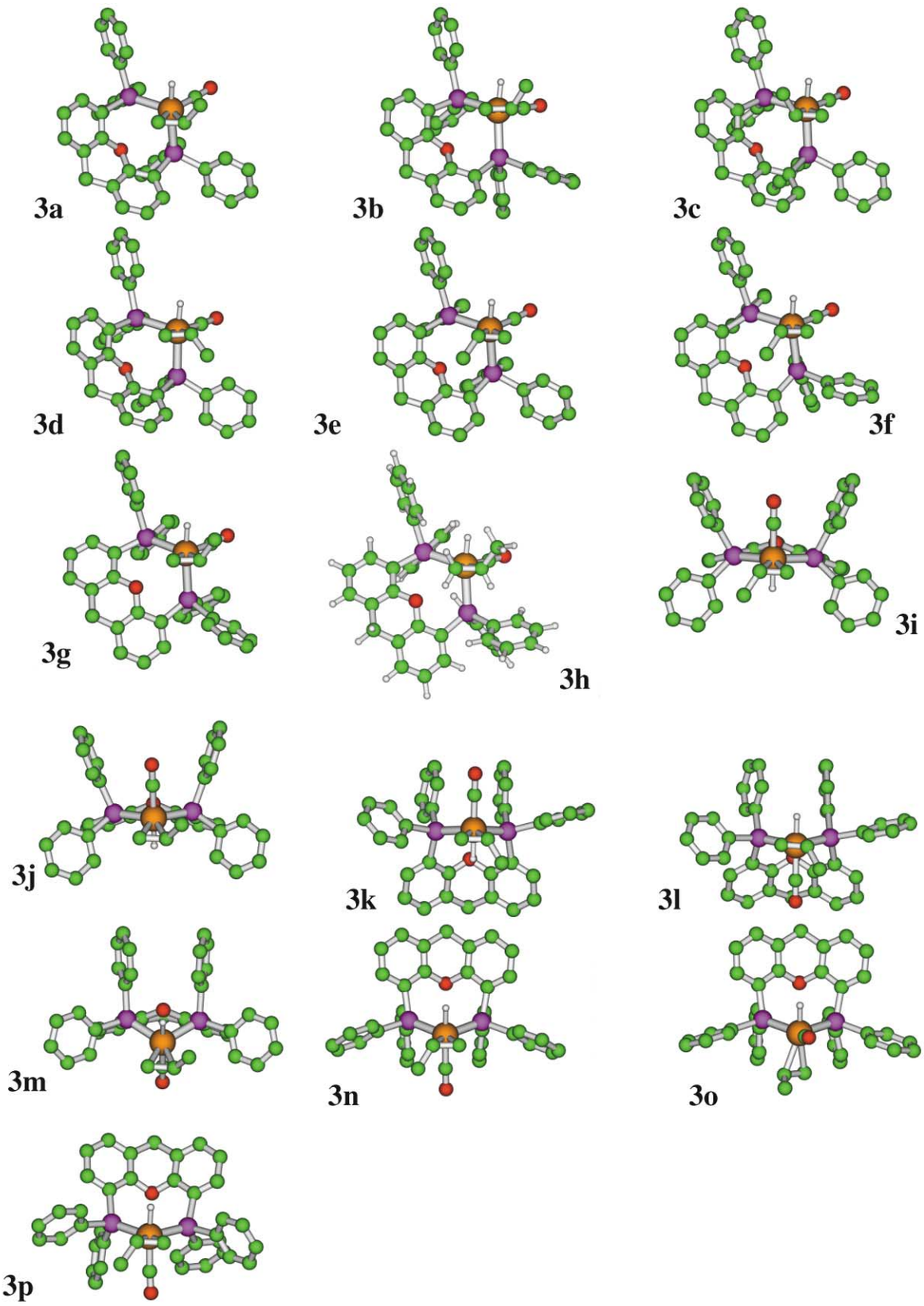

Fig. 5 Structures computed for **3**.

formers, we turn to the barriers associated within isomers and the barriers for reaction to form subsequent intermediates (Table 8).

Isomerization and interchange of complexes 1 and 2

It is generally expected that conformational equilibria will have low barriers to exchange. We have tested this expectation by computing the transition states that connect the proximal conformation of **1a** with the distal conformation of **1d**. As expected the conformational exchange has a small free energy of activation, 4.1 kcal mol^{-1} (relative to **1a** in Table 1), and a low frequency imaginary mode of $-34cm^{-1}$. Axial-equatorial exchange, **1a** $\longrightarrow$ **1c** is computed to occur with a barrier in free energy of 12.5 kcal mol^{-1}, which is just slightly higher than the value of 10.5 kcal mol^{-1} reported by

Table 6 Geometric parameters computed for isomers of **5**

	$Rh–C_{Pr}$/Å	$Rh–C_{CO1}$/Å	$Rh–C_{CO2}$/Å	$Rh–P_1$/Å	$Rh–P_2$/Å	Bite angle/°
5a	2.176	1.926	1.885	2.547	2.548	103.6
5b	2.179	1.926	1.888	2.527	2.536	106.4
5c	2.196	1.925	1.871	2.693	2.549	99.7
5d	2.187	1.906	1.902	2.635	2.544	101.0
5e	2.177	1.903	1.906	2.617	2.526	102.2
5f	2.180	1.903	1.909	2.642	2.546	99.9
5g	2.192	1.912	1.894	2.672	2.558	101.0
5h	2.197	1.989	1.879	2.581	2.581	101.8
5i	2.202	1.928	1.883	2.547	2.547	104.5

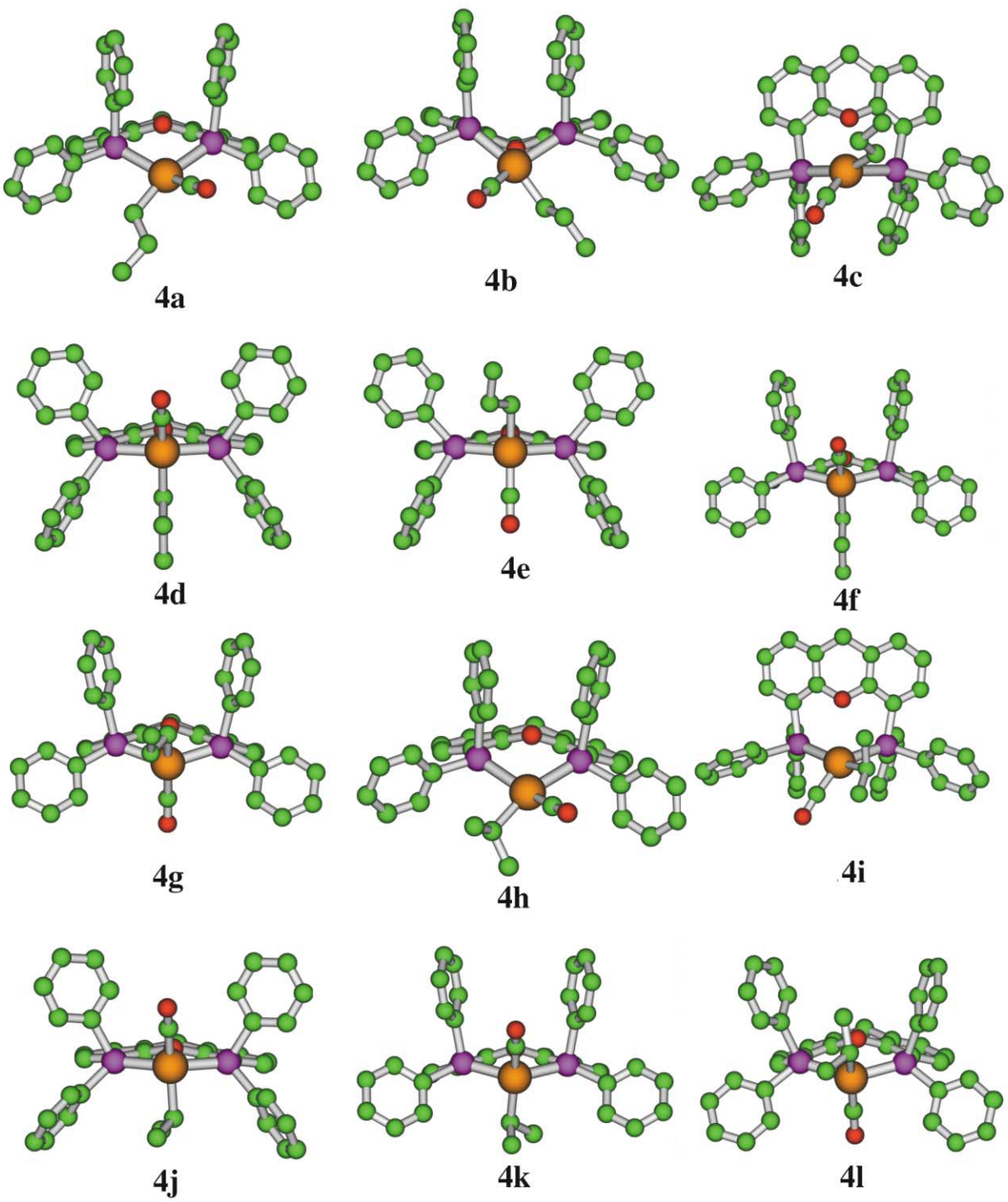

Fig. 6 Computed structures for isomers of **4**.

Castellanos-Páez *et al.*[32] for axial-equatorial exchange in the complex $HRh(BDPP)(CO)_2$ (BDPP = (2*S*,4*S*)-bis(diphenylphosphino)pentane).

Isomers of **2** undergo exchange and conformational transitions with little energetic barrier. For example, the transition state which connects the *cis* isomer **2a** with the *trans* isomer **2e**

Table 7 Geometric parameters computed for isomers and conformers of **6**

Structure	Rh–H/Å	Rh–C/Å	Rh–P1/Å	Rh–P2/Å	Bite angle/°
6a	2.011	1.844	2.627	2.558	103
6b	1.992	1.849	2.583	2.550	104
6c	2.015	1.844	2.592	2.569	103
6d	2.055	1.915	2.381	2.382	132
6e	1.995	1.848	2.595	2.557	104
6f	2.069	1.915	2.387	2.390	132

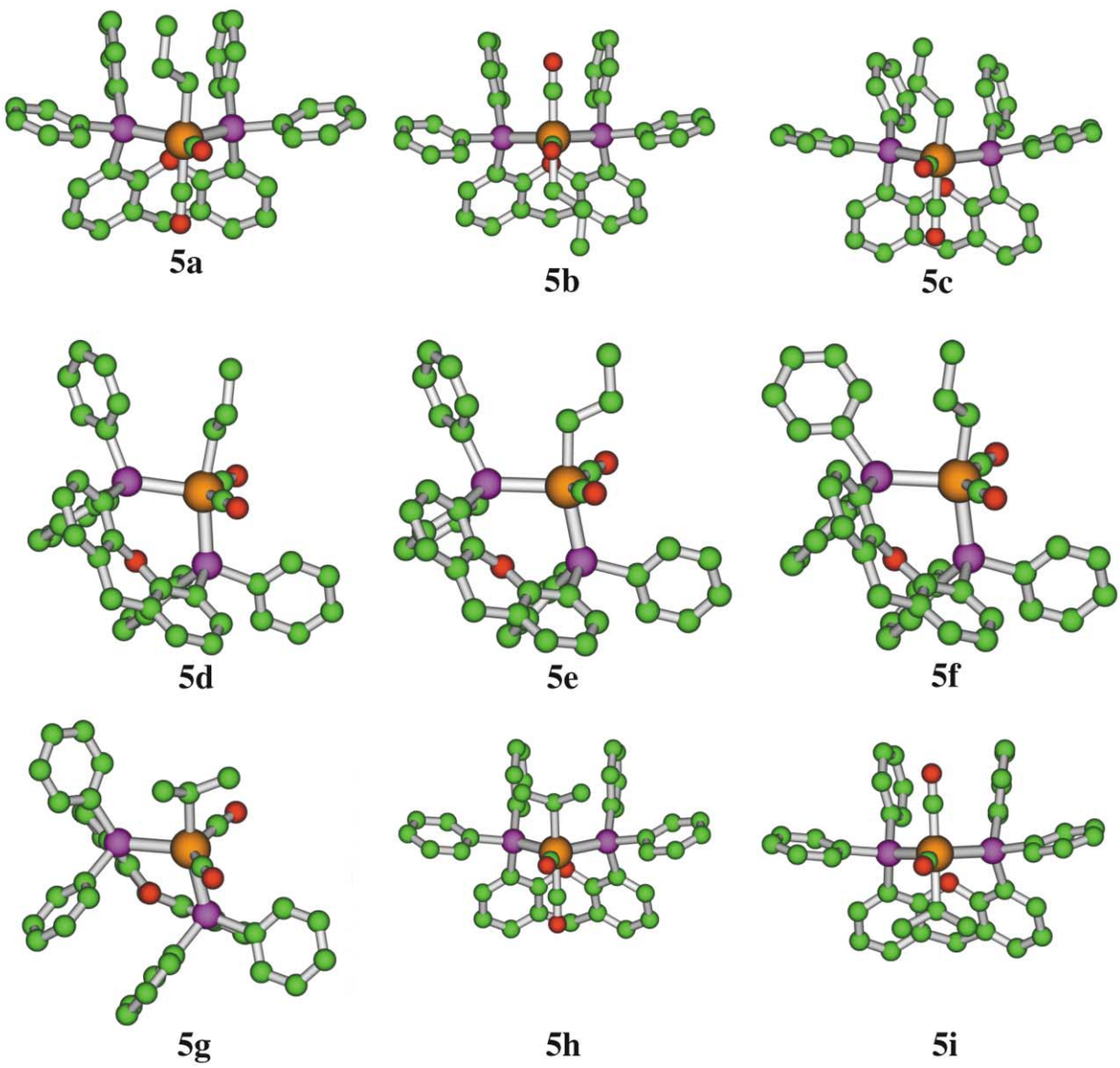

Fig. 7 Computed structures for **5**.

lies just 5.5 kcal mol^{-1} higher in free energy than **2a**. Similarly, the proximal ⟶ distal conformational conversion which converts **2a** into **2b** traverses a free energy barrier of just 2.3 kcal mol^{-1}.

Dissociation of CO from **1a** to form **2a** is a barrierless process. The lowest energy trajectory for CO loss involves significant bending of the Rh–C–O angle as the CO dissociates. This type of trajectory has been identified previously in Krogh-Jespersen *et al.*'s[33] computations of CO dissociation from Ir complexes. Because we find a barrierless process, the kinetics of CO dissociation can be estimated from the relative free energies of **1a** and **2a**. The free energy difference of 15.1 kcal mol^{-1} based on gas phase computations at 298 K compares reasonably with experimental values of 20 kcal mol^{-1} [14] for CO dissociation in closely related complexes derived from ^{13}CO exchange measurements in solution at 40 °C. This important reference point is one of the few good opportunities to directly compare relevant experimental and empirical data. Based on this assessment it appears that the ONIOM model performs reasonably for a gas phase simulation of a solution process.

Formation and fluxional processes of complex 3

Association of propene with **2** yields the trigonal bipyramidal isomers of **3**. Recall that the thermodynamic free energies of these association reactions cluster around 0 kcal mol^{-1}. We have located six transition states for these processes. Four of the transition states take isomer **2a** to the isomers **3a**, **3c**, **3d**, and **3e**. The other two connect the isomer **3j** with **2b** and **2d**. Whereas association of CO has no computed barrier, our computations

Table 8 Transition state energies computed for various processes relative to **2a**

	$\Delta H°^a$	$\Delta G°^a$	$\Delta S°^b$	ΔE^a	Imaginary frequency i/cm^{-1}
1 ⟶ **1** isomerization					
1a ⟶ **1c**	−14.09	−2.64	−38.41	−14.32	−410
1a ⟶ **1d**	−23.09	−10.98	−40.61	−23.93	−34
2 ⟶ **2** isomerization					
2a ⟶ **2e**	5.03	5.47	−1.49	5.87	−196
2a ⟶ **2b**	1.65	2.33	−2.26	2.23	−58
3 ⟶ **3** isomerization					
3l ⟶ **3l**	9.67	22.96	−44.56	8.65	−29
3c ⟶ **3n**	21.13	34.73	−45.60	20.83	−385
2 ⟶ **3** transition states					
2b ⟶ **3g**	4.77	17.09	−40.58	4.02	−82
2a ⟶ **3a**	5.63	18.89	−41.33	4.78	−71
2a ⟶ **3d**	5.94	19.30	−44.47	5.13	−73
2a ⟶ **3e**	5.50	18.74	−44.83	4.71	−71
2a ⟶ **3c**	6.42	18.84	−44.42	5.61	−69
2d ⟶ **3j**	6.42	18.84	−41.65	5.61	−68
3 ⟶ **4** transition states					
3n ⟶ **4e**	17.48	31.64	−47.50	16.98	−764
3a ⟶ **4f**	12.07	26.53	−48.51	11.85	−719
3j ⟶ **4a**	13.69	27.81	−47.37	13.23	−645
3 ⟶ **4i** transition states					
3a ⟶ **4k**	20.81	34.89	−47.23	20.60	−946
3n ⟶ **4k**	15.32	29.25	−46.72	14.77	−766
3a ⟶ **4h**	18.92	33.73	−49.66	18.74	−988

[a] kcal mol^{-1} at 298 K. [b] cal mol^{-1} K^{-1}.

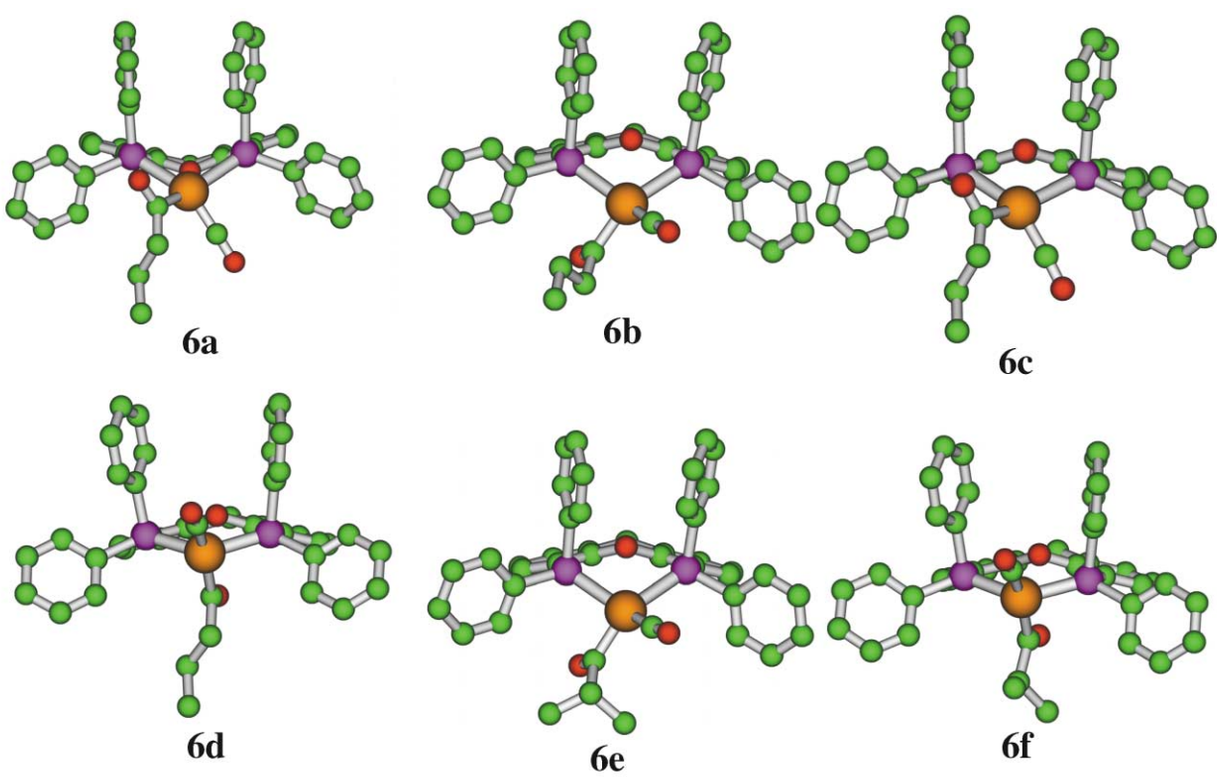

Fig. 8 Computed structures for **6**

consistently yield significant activation free energies for propene association that span a narrow range of 17.1–19.3 kcal mol^{-1}. It appears that the combination of basis sets and ONIOM layers do not suffice to give realistic energies for the interaction of the catalyst with propene, either in the kinetic or thermodynamic sense. Unfortunately we have been unable to find published transition states and energies for alkene association in simpler model systems to compare with our results. Thus, this crucial step in the overall catalytic process will require significantly more attention in future work.

We have examined two fluxional processes at the trigonal bipyramidal isomers of **3**: rotation of the coordinated propene and interconversion of axial-equatorial and diequatorial xantphos coordination modes. Rotation of the propene group at the diequatorial isomer **3l** (transformation **3l** ⟶ **3l** in Table 8) incurs a free energy barrier of 8 kcal mol^{-1} (relative to **3l** in

Table 1) at 298 K. Essentially this is the energy for rotation of the C–C bond vector perpendicular to the equatorial coordination plane. Conversion of the diequatorial isomer **3p** to an axial-equatorial similar to **3b** must cross a free energy barrier of about 20 kcal mol^{-1}. This is a rather high barrier for this exchange process. It remains to be seen if this computation is generally representative of diequatorial/axial-equatorial exchange processes at **3**.

Formation of complex 4

Particularly in the recent work of Carbó *et al.*, attention has been focussed on the transformation **3** ⟶ **4** under the hypothesis that this is the step in which the reaction regioselectivity is fixed. Let us first consider the absolute magnitude of the activation free energies that we compute for insertion of propene into Rh–H bonds. Relative to complex **2a**, the free energies of the seven transition states that we have located so far, four to give *n*-propyl complexes and three to give *i*-propyl complexes, range from 26.5 to 34.9 kcal mol^{-1}. Given that **2a** is neither the computed nor the experimentally observed resting state of the catalyst and given that hydroformylation with these ligands proceeds with turnover frequencies on the order of 100 h^{-1}, the computed insertion transition state free energies are far too high. As mentioned previously, the weak exothermicity computed for binding propene is a major contributor to the large discrepancy between experiment and computation.

Although the sampling of transition states for the transformation of **3** to **4** is still sparse, some interesting trends are seen. The lowest energy pathway (**3a** ⟶ **4f**) for the formation of the *n*-propyl isomers is initiated from an axial-equatorial isomer and yields a *trans* square planar complex. In contrast, the lowest energy pathway (**3n** ⟶ **4k**) yielding an isopropyl isomer converts a di-equatorial five-coordinate complex into a *trans* square planar complex. If one assumes that the ratio of these two lowest energy pathways determines the *n*/*i* ratio of the product aldehyde, one obtains the ratio 42 : 1 at 80 °C. This number, fortuitously, coincides remarkably well with the experimental ratio of 52 : 1 observed for 1-octene hydroformylation with the xantphos-ligated catalyst at 80 °C.[14]

Discussion

Computations play an increasingly important role in understanding the details of catalytic reaction mechanisms. During the past decade the speed and accuracy of modern quantum mechanical (QM) codes as well as the computational power available from clusters based on commodity PC's has grown rapidly. Our first goal for this project is to explore whether attempting realistic QM simulations of the hydroformylation catalytic cycle is reasonable. Based on the sheer magnitude of intermediates, transition states, and their conformers that have been located during the initial stages of this project it is clear that a reasonable exploration is within our reach, even with rather modest resources. Although we have not achieved the level of conformational sampling that could be achieved by dynamics methods, these early results show that a large variety of geometric isomers and conformers can be located using *non*-dynamics methods and, more importantly, must be considered for realistic modelling. This work also amply demonstrates that computational estimates of free energies, a most useful quantity for comparing experimental observations with computational predictions, can be achieved in a reasonable time frame.

Catalytic hydroformylation is an important industrial process that is poorly understood in terms of the detailed reaction mechanisms. A second goal of this work is to gain insights into the reaction mechanism that are not easily obtained from experiment alone. Relevant questions include: Why does a wide bite angle favour normal aldehydes? What is the catalyst resting state? What is the selectivity-determining step of 1-alkene hydroformylation? How could the catalyst be modified to increase activity? What should be the catalyst rate law and why? How do isotopic substitutions affect the reaction rates and why?

Important empirical observations concerning xantphos-based hydroformylation catalysts are reproduced by computations. It is clear from the computations that most of the catalyst will pool in the form of **1**. This species, which is the only observed species under catalytic conditions according to NMR and IR experiments, is computed to populate both axial-equatorial and diequatorial coordination modes of the xantphos ligand.

Experiment also suggests significant population of both isomer classes, although the experimental estimates (7 : 3 ee : ae) differ somewhat from computation (1 : 9 ee : ae). The computed free energies of CO dissociation (15 kcal mol^{-1}) are somewhat lower than experimental estimates (20 kcal mol^{-1}) based on isotopic exchange measurements but are not unreasonable. Computation of the insertion barriers to form *n*-propyl isomers *vs.* *i*-propyl isomers agree with the *n* : *i* aldehyde ratio observed in experimental studies, but this value must be considered fortuitous at this stage due to the egregious errors that are seen in estimates of the overall hydroformylation activity.

Even at the early stages (**3a** ⟶ **4f**) of the hydroformylation reaction, such high free energy barriers (*ca.* 41 kcal mol^{-1}) are computed for taking the catalyst from its resting state (**1a**) to product that any insights into the kinetics of the catalytic process are precluded. It appears that a major culprit is a dramatically underestimated enthalpy of association of propene with **2**. However, it is not clear if other factors also contribute significantly, such as intrinsically high barriers for alkene insertion, *etc*. With such uncertainties in the magnitudes of important thermodynamic and kinetic free energies, it is impossible to meaningfully evaluate which step is selectivity-determining or which step is turnover-limiting. Such evaluations require high confidence in the relative transition state free energies of steps with different molecularities; that level of confidence is not justified.

Why are the estimated activation free energies for catalysis so inconsistent with experiment? At this point it is not certain, but our previous experience with modelling Rh(diphosphine)-catalyzed enamide hydrogenation did demonstrate the need to have high quality basis sets on Rh and P. Another limitation concerns the B3LYP method. As shown by Decker and Cundari,[10] the energy of propene binding to the catalyst in simple model systems changes dramatically when the energies of B3LYP-optimized geometries are evaluated with CCSD(T) methods. To test the influence of basis sets, computational methods, and basis set superposition errors on the relative energies of key intermediates we have performed the computations summarized in Tables 9 and 10.

The data in Table 9 summarize the effect of computational method and basis set on the thermodynamics of **1** ⟶ **2** and **2** ⟶ **3**. The changes in energy for the core ONIOM and total ONIOM energies are consistently close to one another. For the dissociation of CO from **1** to yield **2** the B3LYP and CCSD(T) computations yield similar results, but the BP86 functional and the MP2 method give CO dissociation energies that are much higher than experimental estimates. For the association of propene and **2** to yield **3**, the B3LYP method yields larger exothermicities as the basis set becomes more sophisticated. Thus, consistency with experiment should improve with better basis sets. Again the BP86 method leads to tighter ligand binding than B3LYP. Interestingly, the CCSD(T) computations with LANL2DZ basis functions give a strongly exothermic reaction (*ca.* −14 kcal mol^{-1}) but most of this disappears when basis set superposition error (BSSE) corrections are estimated with

Table 9 Calculated ΔE(**1** ⟶ **2**) (kcal mol^{-1}) and ΔE(**2** ⟶ **3**) (kcal mol^{-1}) at different levels of theory and with different basis sets

Method	ΔE_{opt}	ΔE_{core}
1 ⟶ **2**		
ONIOM(B3LYP/LANL2DZ : HF/LANL2MB)[a]	+27.69	+26.6
ONIOM(BP86/LANL2DZ : HF/LANL2MB)[a]	+35.9	+34.6
ONIOM(CCSD(T)/LANL2DZ : HF/LANL2MB)[c]	+27.2	26.1
ONIOM(MP2/LANL2DZ : HF/LANL2MB)[c]	—	+33.0
2 ⟶ **3**		
ONIOM(B3LYP/LANL2DZ : HF/LANL2MB)[a]	−2.56	−4.6
ONIOM(BP86/LANL2DZ : HF/LANL2MB)[a]	−10.1	−11.9
B3LYP/(Stuttgart and 6-31G)[b,c]	−6.9	—
B3LYP/(Stuttgart and LANL2DZ)[b,d]	7.7	—
ONIOM(CCSD(T)/LANL2DZ : HF/LANL2MB)[e]	−13.9	−15.8
ONIOM(MP2/LANL2DZ : HF/LANL2MB)[e]		−26.1

[a] Full ONIOM optimisation. [b] Full B3LYP optimisation. [c] Rh and P atoms use the Stuttgart basis sets and ECP's as described in the Methods section; the 6-31G basis set is used on all other atoms. [d] Rh and P atoms use the Stuttgart basis sets and ECP's as described in the Methods section; the LANL2DZ basis set is used on all other atoms. [e] Single point calculations using ONIOM(B3LYP/LANL2DZ : HF/LANL2MB) optimised geometries.

Table 10 ΔE (kcal mol^{-1}) and ΔE (kcal mol^{-1}) corrected for basis set superposition errors (BSSE) for **2** ⟶ **3** ((CO)HRh(PH$_3$)$_2$(propene) ⟶ (CO)HRh(PH$_3$)$_2$ + propene)

Method	ΔE	ΔE_{corr}(BSSE)
B3LYP/LANL2DZ[a]	−4.1	−1.4
BP86/LANL2DZ//B3LYP/LANL2DZ	−11.2	−8.7
MP2/LANL2DZ//B3LYP/LANL2DZ	−26.0	−9.0
CCSD(T)/LANL2DZ//B3LYP/LANL2DZ	−16.0	+1.2

[a] Fully optimised.

counterpoise calculations (see Table 10). Such results underscore the inadequacy of the LANL2DZ basis set functions. It is commonly observed that basis set superposition errors become less significant as the quality of the basis sets improve.[34] Thus the next phase of these computations will focus on the application of higher level basis sets for the core part of the ONIOM computation. As always, more levels of sophistication may be needed such as including solvation effects and the use of larger core fragments in the ONIOM model.

An alternative explanation for the unrealistically high activation energies derived from computations is that the computed mechanism is wrong. For example, it is possible that propene binding to the catalyst is preceded by dissociation of one arm of the xantphos chelate from **1**, rather than dissociation of CO. Due to the strain in the xantphos chelate this could provide a lower energy route to creating a sterically uncongested vacant coordination site to bind propene. To test this hypothesis we have performed preliminary computations along this pathway. Our initial results reveal that addition of propene to **1** along this path is still thermodynamically uphill and that higher than realistic activation energies will necessarily result. Thus, it appears that future studies should focus on the computational methods and basis sets used, rather than the exploration of alternate pathways.

Conclusions

The data presented herein represent substantial progress toward comprehensive modelling of the catalytic hydroformylation reaction. Relative to previous computational studies,[8–12] this work demonstrates clearly that consideration of multiple isomers and conformers is *essential* to realistic modelling. For example, these results conclusively dispel the assumption[12] that only diequatorial isomers of the critical intermediate **3** contribute to product formation as the axial-equatorial isomers are essentially isoenergetic. From the computational perspective, this work establishes useful guidelines for the basis sets and methods required for future progress in realistic modelling of hydroformylation. Overall, this work provides the most comprehensive sketch to date of the structural diversity present in realistic models of hydroformylation catalysts. As such, this work will provide a valuable foundation for subsequent studies to be performed at more sophisticated levels of computation.

Are we at the stage where computations can help us to understand turnover-limiting and selectivity-determining steps for highly active catalysts? Realistic modelling requires, firstly, the ability to search large numbers of conformers and isomers all along the catalytic cycle of model catalysts that reflect the steric and electronic characteristics of real catalysts. As these initial results indicate, computations with a realistic scope are feasible. Obtaining reaction energetics with sufficient accuracy to make kinetic distinctions, such as the nature of the turnover-limiting and selectivity-determining steps, presents a far greater challenge. Catalysts that are highly active necessarily are restricted to a small range of activation free energies. For multi-step reactions such as hydroformylation this means that high accuracies are required to determine whether, for example, insertion of propene into a Rh–H bond will be reversible or irreversible under catalytic conditions. At the level of computation utilized in this work, the necessary accuracy of the thermodynamic and kinetic activation parameters has not been achieved. In the case of hydroformylation, another limitation is the paucity of good empirical data that might be used as constraints for some of the reaction steps.

This is not to say that useful, realistic models are out of reach. In recent studies of the mechanism of asymmetric hydrogenation we have shown that strikingly good agreement between experimental and computational energetics can be achieved. Although the work reported herein falls short of our goals, good progress has been made in much of the difficult work (searching conformational and isomer space, obtaining good structures for intermediates and transition states). Furthermore, there are obvious, feasible approaches to improving the computations. Therefore we conclude that a significant first step has been made to understand catalytic hydroformylation reactions. Our future efforts will focus on both improving computational accuracy and expanding the pool of empirical kinetic data relevant to catalytic hydroformylation.

Acknowledgements

Support for this work was provided by the National Science Foundation. The authors wish to thank Mr Chris Pawela for his expert assistance with the computer hardware used in this project.

References

1 For an excellent overview of relevant hydroformylation chemistry see: *Rhodium Catalyzed Hydroformylation*, ed. P. W. N. M. van Leeuwen and C. Claver, Kluwer-CMC, Dordrecht, The Netherlands, 2000 and references cited therein.

2 C. P. Casey and G. T. Whiteker, *Isr. J. Chem.*, 1990, **30**, 299; P. W. N. M. N. van Leeuwen, P. C. J. Kamer and J. N. H. Reek, *Pure Appl. Chem.*, 1999, **71**, 1443; T. J. Devon, G. W. Phillips, T. A. Puckette, J. L. Stavinoha and J. J. Vanderbilt, (to Texas Eastman), *US Pat.*, 4,694,109, 1987.

3 G. Stanley, in *Catalysis of Organic Reactions*, ed. M. G. Scaros and M. L. Prunier, Marcel Dekker, Inc., New York, 1995, p. 363; U. Nettekoven, P. C. J. Kamer, M. Widhalm and P. W. N. M. van Leeuwen, *Organometallics*, 2000, **19**, 4596.

4 J. E. Babin and G. T. Whiteker (to Union Carbide), WO 93/03839, *US Pat.*, 911518, 1992; G. J. H. Buisman, M. E. Martin, E. J. Vos, A. Klootwijik, P. C. J. Kamer and P. W. N. M. van Leeuwen, *Tetrahedron: Asymmetry*, 1995, **6**, 719.

5 K. Nozaki, N. Sakai, T. Nanno, T. Higashijima, S. Mano, T. Horiuchi and H. Takaya, *J. Am. Chem. Soc.*, 1997, **119**, 4413.

6 C. P. Casey, E. L. Paulsen, E. W. Beuttenmueller, B. R. Proft, L. M. Petrovich, B. A. Matter and D. R. Powell, *J. Am. Chem. Soc.*, 1997, **119**, 11817.

7 W. R. Rocha and W. B. de Almeida, *Int. J. Quantum Chem.*, 2000, **78**, 42.

8 R. Schmid, W. A. Herrmann and G. Frenking, *Organometallics*, 1997, **16**, 701.

9 T. Matsubara, N. Koga, Y. Ding, K. G. Musaev and K. Morokuma, *Organometallics*, 1997, **16**, 1065.

10 S. A. Decker and T. R. Cundari, *Organometallics*, 2001, **20**, 2827.

11 D. Gleich, R. Schmid and W. A. Herrmann, *Organometallics*, 1998, **17**, 2141; D. Gleich, R. Schmid and W. A. Herrmann, *Organometallics*, 1998, **17**, 4828; D. Gleich and W. A. Herrmann, *Organometallics*, 1999, **18**, 4354.

12 J. J. Carbó, F. Maseras, C. Bo and P. W. N. M. van Leeuwen, *J. Am. Chem. Soc.*, 2001, **123**, 7630.

13 M. Kranenburg, Y. E. M. van der Burgt, P. C. J. Kamer and P. W. N. M. van Leeuwen, *Organometallics*, 1995, **14**, 3081.

14 P. W. N. M. van Leeuwen, C. P. Casey and G. T. Whiteker, in *Rhodium Catalyzed Hydroformylation*, ed. P. W. N. M. van Leeuwen and C. Claver, Kluwer-CMC, Dordrecht, The Netherlands, 2000, ch. 4; L. A. van der Veen, P. C. J. Kamer and P. W. N. M. van Leeuwen, *Organometallics*, 1999, **18**, 4765.

15 M. Svensson, S. Humbel, R. D. Froese, T. Matsubara, S. Sieber and K. Morokuma, *J. Phys. Chem.*, 1996, **100**, 19357.

16 S. Humbel, S. Sieber and K. Morokuma, *J. Chem. Phys.*, 1996, **105**, 1959.

17 R. D. J. Froese and K. Morokuma, in *Encyclopedia of Computational Chemistry*, ed. P. v. R. Schleyer, Wiley, New York, 1998.

18 S. Dapprich, I. Komaromi, K. S. Byun, K. Morokuma and M. J. Frisch, *THEOCHEM*, 1999, **462**, 1.

19 M. J. Frisch, G. W. Trucks, H. B. Schlegel, G. E. Scuseria, M. A. Robb, J. R. Cheeseman, V. G. Zakrzewski, J. A. Montgomery Jr., R. E. Stratmann, J. C. Burant, S. Dapprich, J. M. Millam, A. D. Daniels, K. N. Kudin, M. C. Strain, O. Farkas, J. Tomasi, V. Barone, M. Cossi, R. Cammi, B. Mennucci, C. Pomelli, C. Adamo, S. Clifford, J. Ochterski, G. A. Petersson, P. Y. Ayala, Q. Cui, K. Morokuma, D. K. Malick, A. D. Rabuck, K. Raghavachari, J. B. Foresman, J. Cioslowski, J. V. Ortiz, B. B. Stefanov, G. Liu, A. Liashenko, P. Piskorz, I. Komaromi, R. Gomperts, R. L. Martin, D. J. Fox, T. Keith, M. A. Al-Laham, C. Y. Peng, A. Nanayakkara, C. Gonzalez, M. Challacombe, P. M. W. Gill, B. Johnson, W. Chen, M. W. Wong, J. L. Andres, C. Gonzalez, M. Head-Gordon, E. S. Replogle and J. A. Pople, Gaussian 98, Revision A.7, Gaussian, Inc., Pittsburgh, PA, 1998.

20 R. G. Parr and W. Wang, *Density-Functional Theory of Atoms and Molecules*, Oxford University Press, New York, 1994.

21 R. Neumann, R. H. Nobes and N. C. Handy, *Mol. Phys.*, 1996, **87**, 1.

22 A. D. Becke, *Phys. Rev. A*, 1988, **38**, 3098; A. D. Becke., *J. Chem. Phys.*, 1993, **98**, 5648.

23 C. Lee, W. Yang and R. G. Parr, *Phys. Rev. B*, 1988, **37**, 785.

24 P. J. Hay and W. R. Wadt., *J. Chem. Phys.*, 1985, **82**, 299.

25 P. J. Hay and W. R. Wadt, *J. Chem. Phys.*, 1985, **82**, 285.

26 T. H. Dunning and P. J. Hay, in *Modern Theoretical Chemistry*, ed. H. F. Schaefer III, Plenum, New York, 1976, vol. 3, p. 1.

27 W. J. Hehre, R. F. Stewart and J. A. Pople, *J. Chem. Phys.*, 1969, **51**, 2657.

28 D. Andrae, U. Haeussermann, M. Dolg, H. Stoll and H. Preuss, *Theor. Chim. Acta*, 1990, **77**, 123–141.

29 A. Bergner, M. Dolg, W. Kuenchle, H. Stoll and H. Preuss, *Mol. Phys.*, 1993, **80**, 1431–1441.

30 S. Huzinaga, *Gaussian Basis Sets for Molecular Calculations*, Elsevier, Amsterdam, 1984.

31 R. Ditchfield, W. J. Hehre and J. A. Pople, *J. Chem. Phys.*, 1971, **54**, 724–728; W. J. Hehre, R. Ditchfield and J. A. Pople, *J. Chem. Phys.*, 1972, **56**, 2257–2261; P. C. Hariharan and J. A. Pople, *Theor. Chim. Acta*, 1973, **28**, 213–222; P. C. Hariharan and J. A. Pople, *Mol. Phys.*, 1974, **27**, 209–214.

32 A. Castellanos-Páez, S. Castillón, C. Claver, P. W. N. M. van Leeuwen and W. G. J. de Lange, *Organometallics*, 1998, **17**, 2543.

33 F. Abu-Hasanayn, K. Krogh-Jespersen and A. S. Goldman, *J. Am. Chem. Soc.*, 1994, **116**, 5979.

34 K. A. Peterson and T. H. Dunning, *J. Chem. Phys.*, 1995, **102**, 2032.